HHS Public Access

Author manuscript

Dev Biol. Author manuscript; available in PMC 2016 May 15.

Published in final edited form as:

Dev Biol. 2015 May 15; 401(2): 249–263. doi:10.1016/j.ydbio.2015.01.028.

The dynamics of plus end polarization and microtubule assembly during Xenopus cortical rotation

David J. Olson, **Denise Oh**, and **Douglas W. Houston**

The University of Iowa, Department of Biology, 257 BB, Iowa City, IA 52242-1324, USA

Douglas W. Houston: douglas-houston@uiowa.edu

Abstract

The self-organization of dorsally-directed microtubules during cortical rotation in the Xenopus egg is essential for dorsal axis formation. The mechanisms controlling this process have been problematic to analyze, owing to difficulties in visualizing microtubules in living egg. Also, the order of events occurring at the onset of cortical rotation have not been satisfactorily visualized in vivo and have been inferred from staged fixed samples. To address these issues, we have characterized the dynamics of total microtubule and plus end behavior continuously throughout cortical rotation, as well as in oocytes and unfertilized eggs. Here, we show that the nascent microtubule network forms in the cortex but associates with the deep cytoplasm at the start of rotation. Importantly, plus ends remain cortical and become increasingly more numerous and active prior to rotation, with dorsal polarization occurring rapidly after the onset of rotation. Additionally, we show that vegetally localized Trim36 is required to attenuate dynamic plus end growth, suggesting that vegetal factors are needed to locally coordinate growth in the cortex.

Keywords

egg; oocyte; polarity; microtubules; axis formation; plus ends; Xenopus; cortical rotation; Trim36

Introduction

The differential localization specific proteins, mRNAs, and cellular organelles is a fundamental mechanism for establishing cell polarity. In oocytes and eggs, these processes are often essential for subsequent egg development and for cell fate specification and tissue patterning during development. One striking example of cytoplasmic localization in the fertilized amphibian egg is the wholesale rotation of the egg cortex about the deep cytoplasmic core during the first cell cycle. This cortical rotation results in the establishment of dorsoventral asymmetry by enriching putative dorsal determinants on the future dorsal side of the early embryo, triggering the activation of Wnt/β-catenin signaling (reviewed in

Correspondence to: Douglas W. Houston, douglas-houston@uiowa.edu.

Weaver and Kimelman, 2004; Gerhart, 2004; Houston, 2012). Cortical rotation critically depends on the self-organized assembly and polarization of dorsally directed parallel microtubule arrays. These arrays form in the subcortical region of the fertilized egg at a fluid interface (shear zone) between the cortex and cytoplasmic core. The functions of this assemblage of microtubules in axis formation is thought to be two-fold: first to facilitate the large-scale movement of the cortex over the deeper cytoplasm, and second to orient the dorsally-directed transport of putative dorsalizing molecules/organelles along the array by kinesin-related motor proteins (reviewed in Weaver and Kimelman, 2004; Gerhart, 2004; Houston, 2012).

Recent studies have identified unsuspected roles for mRNAs that are vegetally localized during oogenesis in controlling cortical rotation and vegetal microtubule array assembly (reviewed in Houston, 2012). Antisense-mediated knockdown of maternally localized *perilipin 2* (*plin2/fatvg;* (Chan et al., 2007)) and *tripartite motif containing 36* (*trim36;* Cuykendall and Houston, 2009) resulted in ventralized embryos that failed to undergo microtubule assembly and cortical rotation. Trim36 encodes a RING finger-containing ubiquitin ligase, and microtubule assembly was dependent on Trim36 ubiquitylation activity. Mei et al. (2013) showed that the RNA-binding protein Dead end homolog 1 (Dnd1), also encoded by a localized mRNA, anchors *trim36* mRNA vegetally, thereby concentrating Trim36 activity at the cortex. The regulation of Trim36 and its specific ubiquitylation targets are unknown. Additionally, localized mRNAs have been implicated in regulating the correlate of cortical rotation in zebrafish. Although teleost fish eggs are suspected to lack typical cortical rotation (translocation of the cortex relative to deep cytoplasm), microtubule-dependent cytoplasmic localizations that result in dorsal Wnt/β-catenin signaling have been observed in zebrafish and medaka zygotes (Jesuthasan and Stähle, 1997; Trimble and Fluck, 1995; Strähle and Jesuthasan, 1993). Asymmetrically-oriented microtubules have recently been characterized in the vegetal cortex of zebrafish fertilized eggs (Tran et al., 2012) and a number of vegetally-localized proteins and mRNAs have been shown to undergo an off-center shift from the vegetal pole of the teleost egg following fertilization, in a microtubule-dependent manner. Among these are *wnt8* (Lu et al., 2011) and the gene products of ventralized maternal-effect zebrafish mutants *tokkaebi* and *hecate,* encoding Syntabulin and Grip2a proteins, respectively (Nojima et al., 2010; Ge et al., 2014). Both proteins are suspected to act in the transport of vesicles, and in the case of *hecate,* microtubule assembly is disrupted (Ge et al., 2014). Together, these data demonstrate that vegetal microtubule array assembly is a conserved feature of development, which is controlled in part by factors encoded by localized mRNAs.

Despite the importance of microtubule-dependent cortical rotation in dorsal axis formation, the molecular mechanisms involved in the organization and orientation or cortical microtubules are not fully understood. The most widely favored model for the orientation of the array is a positive feedback mechanism whereby initial stochastic asymmetry in microtubule growth is further amplified by ongoing movement of the cortex (Gerhart et al., 1989; Gerhart, 2004). Microtubules growing in the cortex, originating either from the sperm aster or from within the cortex itself are thought to provide the initial movement cue (Houliston and Elinson, 1991; Schroeder and Gard 1992). Cortical movement then serves to

progressively stabilize microtubule growth or formation in the same direction, either by a "combing" mechanism mediated by cortically anchored kinesin-related proteins (Marrari et al., 2003; Weaver and Kimelman, 2004) or by shear-induced alignment of microtubule-stabilizing endoplasmic reticulum and vesicles (reviewed in Gerhart, 2004). Although the feedback model is compelling and likely correct in the broad sense, the behavior and directionality of individual microtubules undergoing alignment has never been observed to provide direct corroborating evidence.

Observing microtubule dynamics in living Xenopus oocytes and eggs using traditional microtubule probes has proven notoriously difficult (e.g., see Mandato and Bement, 2003), owing to the large excess of tubulin subunits and relative lack of inducible microtubule polymerization (Mandato and Bement, 2003; Jessus et al., 1987; Gard and Kirschner, 1987). Previous studies have visualized cortical microtubules using injection of fluorescently labeled tubulin protein (Houliston, 1994; Larabell et al., 1996). However, it is problematic to image the earliest stages of microtubule assembly and quantitatively measure microtubule dynamics using this approach. The behavior of GFP-Krt8 (Ck1(8)) has been observed throughout cortical rotation (Clarke and Allan, 2003), and while cytokeratin filaments form into parallel arrays (Klymkowsky et al., 1987; Clarke and Allan, 2003), this assembly follows that of microtubules. Consequently, the behavior of microtubules in vivo and their orientation during the pre- and peri-initiation phases of cortical rotation have remained obscure.

Here, we characterize total microtubule and plus-end dynamics in Xenopus oocytes and eggs and begin to investigate the roles of localized mRNA gene products in this process. We identify changes in microtubule stability and plus end flux during the oocyte-to-egg transition. Furthermore, we observed several new behaviors occurring at the onset of cortical rotation, including chaotic plus end motion and a subsidence of the nascent microtubule array into deeper layers. By tracking plus end directionality, we follow the progression of dorsal orientation of microtubules during cortical rotation and correlate this with the onset of relative cortical movement and changes in plus end growth length. Last, we show that Trim36 acts to coordinate plus end growth by differentially modulating growth speed and stability. Overall, these data provide a framework for routine and quantitative analysis of microtubule assembly in the oocyte and developing egg.

Results

Differential regulation of microtubule and plus end stability during the oocyte-to-egg transition in *Xenopus*

To begin to characterize microtubule assembly and dynamics in the developing *Xenopus* egg, we first examined cultured oocytes expressing microtubule and plus end fluorescent fusion proteins. Of various approaches we initially evaluated, neither injection of fluorescent tubulin protein, tubulin-binding drugs, nor injection of *gfp-tubulin* or *tau-gfp* mRNAs produced consistent results. We were able to visualize microtubules and plus ends in oocytes by injecting mRNAs encoding multimers of the Ensconsin/Map7 microtubule-binding domain (EMTB) fused with multimers of GFP or mCherry (Miller and Bement, 2009;

EMTB-3xGFP/2x mCherry; doses ~ 500 pg), and mRNAs encoding EB3- GFP (500 pg), respectively.

Examination of *emtb-gfp*-injected oocytes revealed a meshwork of labeled microtubules throughout the cortex (>100 oocytes; 95% of cases, Fig. 1A). Distinct foci were also seen, either isolated or at the intersection of microtubules in the network. This labeling pattern disappeared when oocytes were incubated in the cold (data not shown) or treated with nocodozole (3.3 μM, Fig. 1B), verifying that EMTB-GFP was indeed marking microtubules. Similar results were seen for EMTB-mCherry (Fig. 1F). Short time-lapse videos showed that the EMTB-labeled microtubules were stable, displaying random swaying movements but lacking dynamic activity (Supplementary Video 1). Because biochemical evidence has shown that a pool of stable microtubules becomes depolymerized during the oocyte-to-egg transition (Jessus et al., 1987; Gard and Kirschner, 1987; Elinson, 1985), we next followed changes in EMTB-labeled microtubule organization during oocyte maturation. Consistent with biochemical observations, EMTB-GFP labeling in the cortex became markedly reduced following overnight progesterone treatment (Fig. 1D). Prick activation of these mature eggs resulted in complete loss of EMTB-GFP labeled microtubules, which did not become evident again until the beginning of cortical rotation (see below).

Injection of *eb3-gfp* mRNA (~ 500 pg; alone or along with *emtb-mCherry*) resulted in labeling of numerous plus ends in the cortex (Fig. 1E–H). In our hands these structures were only clearly visible using high numerical aperture oil immersion objectives (60X–100X; N.A. = 1.4). In short time-lapse videos, EB3-labeled plus end “comets” were short-lived, highly dynamic and grew in random directions in the plane of the cortex of the oocyte (Supplementary Video 1). This level of dynamic activity was somewhat surprising considering the general stability of oocyte microtubules. However, these plus ends do no appear to generate microtubules behind them, which is generally consistent with global inhibition of microtubule assembly in oocytes by unknown mechanisms (Gard and Kirschner, 1987; Govindan and Vale, 2000). Because of the dramatic changes in stable microtubules following oocyte maturation, we also examined microtubule plus ends in progesterone-treated oocytes (eggs; Fig. I–L, Supplementary Video 2). Compared to oocytes, plus ends in eggs were less numerous and dynamic. Instead of rapid fluxing, plus ends in eggs appeared more stable and appeared to oscillate back and forth or undergo long, slow growth phases.

To better quantify the dynamics of these microtubule behaviors, we performed automated tracking of EB3-GFP-labeled plus ends in time-lapse images using an established open source software package (plusTipTracker; Applegate et al., 2011). This method directly monitors microtubule growth phases, during which EB3 and other plus end-binding proteins associate with the growing microtubule end. Other aspects of microtubule dynamics including transitions between pausing and shrinking can be computationally inferred from the growth tracks (Matov et al., 2010).

Images of EB3-labeled plus ends were collected from oocytes injected with *eb3-gfp* and/or *emtb-mCherry*, either untreated or progesterone-treated. Plus end comets were detected and tracked (Fig. S1). Images were taken at two-second intervals over a period of two minutes.

We tracked over 20,000 total comets in 40 oocytes and eggs obtained from three different females (Table 1). Oocyte plus ends grew at a rate of about 7.0 μm/minute with an average lifetime of about 7.0 seconds, which are on the lower end of estimates for plus end dynamics in cultured cells. Eggs had visibly fewer plus end growths, and tip tracking confirmed this observation. Oocytes had an average of about 350 growth events occurring per minute (per field of observation), whereas this number was reduced more than half in eggs. Plus end growth speed was not markedly different in eggs although growth lifetime was significantly increased (Fig. 2A). Interestingly, other parameters were not significantly changed upon oocyte maturation, including those related to pausing. This observation was inconsistent with the visual behavior seen in time-lapse videos since the oscillatory movements would seem to indicate greater pausing.

To resolve this discrepancy, we manually tracked oscillating plus ends using kymographs in a subset of videos (N=10; Fig. 2B) and (Fig. 2C–D″). Whereas comets in the oocyte always showed steady growth and were never seen to move backwards, those in the egg showed frequent backward translocations, appearing as distinct peaks or series of peaks in the kymograph plot (Fig. 2D–D″). Because plusTipTracker relies on gaps in the growth tracks to infer other behaviors, the pausing and shrinking dynamics may not be accurately reflected in data from eggs. Our data suggest however that the main differences in microtubule plus end dynamics are in the number of growths and the oscillatory behavior in eggs. Taken together, these results show the utility of Map7 and EB3-based probes for studying microtubule dynamics in oocytes and eggs. Furthermore, our data indicate that oocytes exhibit rapid and dynamic plus end growth along with stable polymeric tubulin, whereas eggs have less dynamic plus end flux, which may be associated with lower overall microtubule stability.

Microtubule assembly during cortical rotation in artificially activated oocytes

Having established methods for measuring plus end dynamics during the oocyte-to-egg transition, we next sought to reexamine the dynamics of vegetal microtubule array organization and plus end activity during cortical rotation. Toward this end, we first examined this process in artificially activated eggs derived from oocytes expressing *emtb-3xgfp* and/or *eb3-gfp.* Progesterone-matured oocytes with visible fluorescent protein expression were sorted and prick activated to mimic fertilization. In all cases, EMTB-labeled microtubules and EB3-labeled plus ends were completely eliminated in eggs examined immediately following activation (n = 20; data not shown). This dramatic loss of polymeric tubulin is generally consistent with published biochemical data (Elinson, 1985; Jessus et al., 1987; Gard and Kirschner, 1987) showing reductions in microtubule density during egg activation. This reduction is thus true for plus end growth as well. We next made extended time lapse movies of prick activated oocytes injected with *emtb-3xgfp* or *eb3-gfp* and followed the subsequent polymerization and polarization of cortical microtubules and plus ends (Fig. 3A, B; Supplementary Videos 3,4). Movies were started when labeled microtubules and plus ends first became visible again, ~25 minutes after activation, and were continued until robust parallel arrays had formed (50–60 minutes post-activation; n = 10 movies, frame rate = 10 seconds). This temporal examination identified several distinct

phases and new microtubule behaviors in the assembly of cortical microtubules during cortical rotation.

a) 25–35 minutes post-activation—During this initial phase of microtubule assembly, microtubule density was low initially, but increased rapidly, and microtubules were short and dynamic. Microtubules translocated in the plane of the cortex and exhibited short bursts of growth, often undergoing buckling after growth termination, suggesting a halting of forward momentum. Other microtubules appeared stationary but buckled prior to rapid plus-end growth. We also observed a novel coiling behavior of microtubule minus ends prior to growth, the significance of which is unknown. During this initial phase of microtubule assembly, EB3-GFP-labeled plus ends were sparsely distributed in the cortex and showed transient growth followed by dramatic disassembly of the plus end tip (Fig. S2, also examples occur in the first 4–5 minutes of Supplementary Video 6). Although these events likely represent catastrophe, individual protofilaments are not predicted to be resolvable under our imaging conditions, suggesting that this “starburst” pattern may be unbundling. Microtubules and EB3-labeled comets appear larger in this phase and there was no relative movement between the deep yolk layer and the cortex.

b) 35–45 minutes post-activation—In the second phase of microtubule assembly, polymerization continued to increase rapidly, with numerous microtubules bending and growing throughout the cortex. The microtubule density was extensive and it became problematic to follow individual microtubules. At this time, the microtubules become thinner and the entire network appeared to sink into the deep cytoplasmic layer. Coincident with this subduction of the microtubule array, relative cortical movement became apparent (~ 36 minutes post-activation). The microtubule network remained disordered and moved along with the deep subcortical yolk platelets and associated pigment granules. A subset of superficial granules remained stationary in the cortex (which adheres to the coverslip during imaging and is immobilized in these experiments), thus providing a stable reference point to discern relative translocation. EB3-GFP-labeled comets were more abundant during this time, and appeared more stable, generally persisting for long periods and failing to show dramatic disassembly characteristic of earlier time periods. Additionally, EB3-GFP comets did not sink into the subcortical layer and remained in the cortex. Polarized plus end growth could be seen by 40 minutes post-activation, with comets seen moving over the deep yolk in the opposite direction. This orientation precedes the formation of robust parallel microtubule arrays (~46 minutes).

c) 45–55 minutes post-activation—In the third phase of cortical rotation, the microtubule mesh-work is progressively resolved into a parallel array and overall microtubule density continues to increase. We observed microtubules in each movie that stayed perpendicular to cortical movement. These eventually disappeared, to be replaced by dense bundles of parallel microtubules aligned with the direction of rotation. During this phase, plus ends appeared to reach a steady-state level and the majority were oriented and moving opposite to the direction of the yolk mass.

d) > 55 minutes—In this last phase, microtubule translocation in the deep layer continued. Over time, the thicker microtubule bundles cables became thinner, straighter and more fine-grained, as has been previously observed in fixed samples, particularly on the ventral side (Marrari et al., 2004). This “fine-combed” appearance is suggested to result from the continual action of cortical kinesin-related proteins, straightening out the microtubules as the cortex moves along them (Weaver and Kimelman, 2004). Kinesins could possibly peel apart thicker bundles they translocate along microtubules, resulting in this thinner appearance late in rotation. Although the significance of “waviness” is unclear, this morphology has been correlated with longer, more stabilized microtubules (Mayr et al., 2007). It is thus possible that the grainier appearance of late phase microtubules could result from microtubule destabilization. Regardless, much of the parallel organization is lost towards the end of cortical rotation (90 minutes), consistent with the termination of cortical rotation at the end of the first cell cycle (Schroeder and Gard, 1992; Marrari et al., 2003). EB3-labeled plus ends continued to grow opposite to yolk rotation (toward the presumptive dorsal side) until rotation ceased. At this point, plus ends returned to randomly directed growth and were reduced in number.

Overall, these results are thus in line with previous imaging studies of bulk movement of organelles and other particles (Larabell et al., 1996), which suggest that cortical rotation begins around the midpoint of the first cell cycle (~ 35 minutes post-activation). However, our observation of the internalization of the microtubule network is novel and this may represent a point of commitment for the egg to undergo cortical rotation. Additionally we find that this internalization and the onset of cortical rotation seem to precede the presumptive dorsal orientation of plus ends and the microtubule array.

Dynamic microtubule parameters during cortical rotation in artificially activated oocytes

To quantitatively assess plus end dynamics during cortical rotation, we made a series of short time-lapse movies at ~10 minute intervals during cortical rotation. Images were collected from oocytes injected with *eb3-gfp* and/or *emtb-mCherry* that were progesterone treated and subsequently prick activated. EB3 comets were then tracked at two-second intervals over two-minute-long movies, covering the period from 25–95 minutes post-activation. In each experiment, we imaged several eggs in succession before returning to the first in the sequence for the next time point. This analysis was repeated seven times using oocytes from different females (n=21; ~8 time points per egg; 147 total movies; Table 2), tracking over 120,000 total comets. Selected frames from a representative time-lapse video series are shown in Fig. 4A–E″; videos were taken from the same egg at the indicated time points (see Supplementary Video 5 for a composite of these videos). These videos show similar general patterns similar as the extended movies, however the greater time resolution was more optimal for reconstruction of microtubule growth tracks (Matov et al., 2010). Also, since many thousands of comets were tracked, we were able to perform robust statistical analyses. The general directionality of plus end growth during each video was assessed using angular data obtained from plusTipTracker (Fig. 4A″–E″).

Overall microtubule behavior was broadly similar to what was seen in the longer interval movies; the number of comets increased and plus ends gradually became oriented with

cortical displacement. However, the shorter frame allowed a more detailed visualization of plus end dynamics. During the initial phases (~30 minutes), plus ends grew smoothly and underwent occasional changes in direction, exhibiting characteristic curvature in the plus end tip (arrows in Fig. 4A). Additionally, upon the transition to cortical rotation (~36 minutes, Fig. 4B, B′), plus end motion became more chaotic and jittery before returning to smoother directional growth at later time points (Fig. 4C–E′). To better identify broad patterns of microtubule dynamics throughout cortical rotation and to find parameters that may correlate with the onset of rotation, we analyzed pooled and averaged data from each time point (Table 2; Fig. 4F–H).

The most significant temporal change in plus end behavior was a dramatic increase in the number of plus ends. Numbers per field rapidly increased during the period from 35′–45′ after activation, from 100–200 per two-minute movie to ~500, and remained high throughout rotation (Fig. 4F). Plus end numbers declined slightly towards the end of rotation. This period of rapid plus end nucleation covers the time in which relative cortical rotation begins and likely is related to overall ongoing microtubule polymerization. The speed of plus end growth over cortical rotation also increased, from a mean speed of ~ 8 μm per minute to ~11 μm per minute by 55 minutes (Fig. 4G). In contrast to the increase in numbers, this increase in speed was gradual and did not change abruptly as overall rotation began. The length of growth events also increased during peak cortical rotation, increasing from ~ 1.0 μm to over 1.8 μm (Fig. 4H). Similar (although inverse) changes were seen in shrinkage length (Table 2). Surprisingly, other parameters indicative of increased microtubule dynamicity were not generally altered throughout cortical rotation. We observed a general pattern showing a spike of increased shrinking behavior in the visibly chaotic period preceding the onset of rotation (Table 2, **35 min**), as well as increased shrinking speed and catastrophe probability during peak cortical rotation. These data show that cortical rotation is associated with robust changes in microtubule numbers and growth length, as well as growth speed and shrinking parameters to a lesser extent.

Patterns of microtubule plus end polarization during cortical rotation in artificially activated oocytes

Several studies have indicated that array microtubules are aligned with the plus ends oriented toward the prospective dorsal side. However, the processes that establish this polarization during cortical rotation have not been addressed. To this end, we analyzed the circular distribution of plus end growths and evaluated changes in mean microtubule orientation and overall directionality (Fig. 4A″–E″). Consistent with visual inspection of the movies, plus ends were randomly directed early in cortical rotation and clearly oriented by 45 minutes post-activation. However, these were not strongly directed until 55 minutes post-activation, at which point the majority of growths were within an ~30° window of arc (Fig. 4D″). We measured concentration around the mean by calculating the mean resultant vector length (r), where r=1.0 indicates uniform directionality, as well as the mean angle ($\bar{\phi}$). We also applied the Rayleigh test to determine if the angular values obtained were significantly nonrandom (Batschelet, 1981; Berens, 2009). As anticipated, plus end growth at the later time points (42–54 minutes, Fig. 4C–E″) showed strong evidence of directionality. Samples

at 36 minutes were not significantly concentrated, further suggesting that growth was randomly directed (Fig. 4B–B″).

Interestingly, in this representative video, plus ends at 30 minutes post-activation showed weak evidence of directionality (p = 8.0E-06, Rayleigh test) in a direction approximately opposite to that of eventual plus end orientation and cortical translocation and in the direction of yolk mass movement. Unfortunately, the low resultant vector magnitude at early time points (Fig. A″) precluded an appropriate statistical correlation of the mean angles of early and late time points (Batschelet, 1981). However, this relationship existed in nearly half of the eggs where similar times could be analyzed (3/7 eggs in which the angle at 30 minutes was opposite to the angle at 50 minutes was within ~60°). Thus, early plus end growth may be more biased than previously appreciated and may play a role in determining the initial direction of rotation.

Because cortical movement is predicted to play a role in determining microtubule orientation, we compared the average mean vector length of EB3-labeled plus ends with overall cortical rotation, as measured by relative movement of the yolk mass ventrally (Fig. 5A, B). We obtained this latter value by inverting the images and tracking pigment granules in the deep yolk. Directionality was weak at 25 and 35 minutes before becoming apparent by 45 minutes and strongly oriented by 55 minutes (Fig. 5A). By contrast, movement of pigment granules was already strongly directional by 45 minutes (Fig. 5B). We empirically defined a significant mean vector length as r = 0.3; the 95% confidence intervals of the mean angle reached a minimum as r approached this value (Fig. 5C). These data experimentally demonstrate that cortical displacement not only precedes parallel microtubule organization but also plus end directionality.

To gain potential insight into possible mechanisms that might influence microtubule polarization, we performed a correlation analysis (Fig. 5D) by plotting mean vector length against various dynamic microtubule parameters. The strongest positive correlations were with number of growths and growth length, whereas growths and shrinkage length were negatively correlated. These data suggest that factors determining the direction of microtubule growth during cortical rotation are most likely those related to the regulation of length of microtubule growth or shrinkage, as well as the overall numbers of plus ends.

Microtubule dynamics in normally fertilized eggs

Although prick activation is sufficient to trigger cortical rotation in eggs, sperm entry and fertilization are thought to play a role in initiating this process in normal development. To determine the extent that the microtubule dynamics seen in artificially activated eggs are similar to those in fertilized eggs, we carried out a smaller series of experiments to track microtubules during in vivo cortical rotation (Fig. 6). Because injected mRNAs encoding fluorescent protein reporters after in vitro fertilization do not express visible protein before cortical rotation, we fertilized injected oocytes using the host-transfer procedure (Holwill et al., 1987; Olson et al., 2012). Oocytes were injected with *eb3-gfp* and/or *emtb-mCherry* and treated with progesterone. These were then transferred into the peritoneal cavity of an ovulating female frog, whereupon oocytes enter the oviduct and can be recovered and fertilized in vitro, as with normal eggs. Eggs obtained in this manner thus express reporter

constructs throughout cortical rotation in vivo. Over-expression of these proteins did not affect overall development, as embryos derived from *eb3-gfp/emtb-mCherry*-injected oocytes developed into normal tailbud stage embryos (Fig. S3). To gain a continuous profile of microtubule behavior in these eggs, we generated longer time-lapse videos using a frame rate of two second. This analysis was done on two eggs each using donor oocytes from two different females. EB3-labeled plus ends were tracked in one-minute intervals using plusTipTracker and temporally analyzed (Fig. 6).

Overall, the microtubule parameters and general patterns of microtubule array assembly and plus end orientation we obtained in vivo were strikingly similar to the data from prick-activated oocytes. Relative cortical displacement could be seen by ~36 minutes post-fertilization, with plus end orientation becoming apparent from 38 – 42 minutes and dense parallel bundles of microtubules forming by ~46 minutes (Fig. 6A). We also saw similar increases over time in mean number of growths, growth speed and growth length in fertilized eggs as in activated ones (Fig. 6C–E). These data thus suggest that the broad patterns of microtubule assembly are similar in cases of fertilization by sperm and artificial activation, and that the latter be used effectively to study cortical rotation mechanisms.

Trim36 coordinates plus end growth and microtubule assembly during cortical rotation

We next examined microtubule dynamics in eggs depleted of maternal Trim36, which we previously showed was essential for vegetal microtubule assembly and axis formation (Cuykendall and Houston, 2009). We injected oocytes with antisense oligos against *trim36* mRNA, followed 24 hours later by injection of *emtb-mCherry* and *eb3-gfp* mRNAs. These oocytes were then matured and prick-activated for time-lapse imaging. A subset of sibling oocytes were fertilized following host transfer and recovery from ovulating host females. Embryonic phenotypes were assessed to confirm that depletion of *trim36* was sufficient cause axis defects (Fig. 7A, D). Microtubule growth and polymerization were similar in control and *trim36*-depleted eggs through the early phases of cortical rotation and the "subduction" of the nascent microtubule network into the deeper yolk appeared to occur normally. However, relative cortical displacement did not initiate in *trim36*-depleted embryos as in controls (Fig. 7B, E, Supplementary Videos 7, 8) and robust parallel arrays did not form. Additionally, plus end numbers were reduced by about half in *trim36*-depleted eggs (1293 ± 95 v. 453 ± 249; $p < 0.005$) and began to exhibit a jittery chaotic behavior beginning around 35 minutes post-activation and continuing into later stages (Fig. 7C, F, Supplementary Videos 7, 8). Numerous episodes of rapid pivots in direction and rearward translocations were evident in *trim36*-deficient eggs but never seen in controls. This chaotic motion continued in later time points but began to diminish by 75 minutes (not shown). Tracking of plus ends confirmed that growth was non-directional in *trim36*-depleted eggs ($r < 0.1$ at all time points; Fig. 7G), which correlates with lack of cortical rotation. Additionally, quantitation of microtubule dynamic parameters identified significant changes in mean growth speed and lifetime, (Fig. 7H) with plus ends growing more rapidly, but for a shorter duration in *trim36*-deficient eggs. Overall, these data suggest that Trim36 might act near the onset of cortical rotation to control growth at the plus end, along with controlling overall microtubule stability.

Discussion

Microtubule-mediated cortical rotation is necessary for establishing embryonic dorsoventral polarity in the amphibian egg. Studies on the assembly and orientation of vegetal cortical microtubules have been limited by the difficulties in visualizing and quantifying microtubule dynamics in live eggs during cortical rotation. We have optimized several of the conditions for following the behavior of microtubule and plus end probes in oocytes and eggs and during cortical rotation. Additionally, we have combined these analyses with loss-of-function of Trim36, a localized tripartite motif-containing protein essential for cortical rotation and dorsal axis formation (Cuykendall and Houston, 2009). This work demonstrates a robust and reliable system for microtubule analysis throughout the oocyte-to-egg-to-embryo transition. Future experiments should allow further characterization of the molecular mechanisms of cortical rotation.

We first worked out the conditions for plus end analysis in full-grown Xenopus oocyte and eggs. We find that the cortex has numerous plus ends growing and disappearing in rapid flux. The role of these growth events is unclear. They may help to replenish microtubules over time since oocytes are held in long periods of quiescence. Additionally, the surface of the oocyte is very active and these plus ends could be involved in transport of structures in the cortex, such as endo- and exocytic vesicles, to which plus ends associate (Pierre et al., 1992). Following oocyte maturation, most of the tubulin is depolymerized and plus ends become much less numerous. The remaining microtubules show changes in behavior, undergoing slower and more sustained growth, as well as undergoing oscillatory plus end motions. These changes could reflect an overall loss of secretion and endocytosis observed in Xenopus eggs. It will be interesting to determine the extent of plus end-mediated vesicle transport in oocytes in future investigations.

Once the egg is activated, the remaining polymeric tubulin is lost and we no longer observe plus end growths. In both prick-activated and fertilized eggs, this is followed by a gradual spontaneous nucleation of microtubules and plus ends beginning around 25 minutes post-activation. Microtubules actively grow and undergo a variety of wriggling, undulating and translocation behaviors. There is frequent buckling prior to growth in this phase, and a curling of the apparent minus end. This novel behavior is of unknown significance. The cortex appears to be the primary site of microtubule nucleation and growth in these experiments. It has been suggested that radial microtubules growing into the cortex from the deep cytoplasm, including those from the sperm aster in fertilized eggs, bend and continue in the cortical plane (Houliston and Elinson, 1991). While our data do not directly address this, we did find distinct points of EMTB- and EB3-GFP accumulation that could represent points of microtubule contact with the cortex or unproductive growth events. However, we also observed plus ends and short microtubule bundles growing and moving locally within the cortex.

The most dramatic and significant event in the egg regarding axial polarization is the robust alignment and dorsal orientation of microtubules associated with cortical rotation. Our results are the first to provide an early and continuous picture of microtubule dynamics at the onset of cortical rotation. These data fit well with the prevailing model for alignment of

microtubules in which cortical movement aligns microtubules. Overall however, we find that alignment of plus ends occurs fairly rapidly after the onset of rotation as opposed to a more gradual refining over time. We also identify several novel features of the self-organizing process that are only apparent upon live imaging of microtubule dynamics.

First, we show that detectable plus end asymmetry indeed becomes evident slightly after the onset of bulk cortical rotation, which occurs at around 36 minutes post-activation/fertilization, in agreement with previous studies (Larabell et al., 1996). Plus ends become detectably polarized by 38 minutes, whereas significant polarity and parallel organization of microtubules is not apparent until about 45 minutes after fertilization. These data thus provide direct evidence for the hypothesis that the polarization of microtubules directly follows the onset of cortical movement. In addition, we find that dorsal orientation of plus ends happens rapidly and precedes the parallel alignment of the majority of microtubules. We show that cortical motion orients the plus ends rather rapidly and that the parallel arrays form by new growth rather than by changing the orientation of existing microtubules. Additionally, the number of growing plus ends increases dramatically during this period from 38–42 minutes post-fertilization, indicating that the bulk of parallel microtubules appearing later are derived from new growth in the direction of rotation. These data thus suggest the existence of a co-aligned cue, possibly ER or vesicles, or even simple fluid shear as an polarizing mechanism as opposed to “combing” or physical wrenching of existing microtubules into alignment.

In support of this idea, shear-induced shortening of microtubules has traditionally been used experimentally to induce growth and dynamic instability (Mitchison and Kirschner, 1984). Thus microtubules oriented perpendicularly to rotation might be broken down, serving as new sites for growth, whereas ones aligned in parallel would experience less shear and persist longer. It is possible that this phenomenon may underlie the increase in plus end numbers and dynamicity in the cortex (see below). Total polymeric tubulin assembly in the egg peaks by 45 minutes post-fertilization (Elinson, 1985) whereas our data suggest that in the cortex, plus ends and dynamic events continue to increase until about 65 minutes. These events may be cortical-specific events driven by the rotation itself rather than reflecting a general tendency towards microtubule polymerization in the fertilized egg. Formally however, it is not known if the subcortical shear forces are of sufficient magnitude to cause microtubule shortening.

Second, we show a novel internalization (microtubule subduction) of the microtubule array as relative cortical displacement begins, concomitant with a more chaotic movement of plus ends. The plus ends remain in the cortex and become more numerous. This microtubule internalization phenomenon could represent an increased association of microtubules with the cytoplasmic core and/or the formation of the so-called fluid “shear zone” which facilitates relative motion between the two layers. Since mechanical perturbations of cortical rotation (e.g., gravity, cold, ultraviolet irradiation) are more effective prior to the time when microtubule subduction would occur, this could represent a commitment to undergo rotation. The jittery movements of plus ends may represent a buildup of cytoskeletal tension in the cortex, which is then released following the formation of the shear zone. It is unclear if microtubule subduction is related to the thickening of the actin cortex following fertilization.

This is unlikely to have a direct role. Cortical thickening would happen prior to subduction, within 30 minutes of fertilization (Charbonneau and Picheral, 1983; Hebard and Herold, 1983). Also, cortical rotation can occur if cytochalasin is applied during this time frame (Elinson and Manes, 1978; Vincent et al., 1987), although we have not examined subduction under these conditions.

Third, assessment of microtubule dynamics indicates that measurements of dynamicity generally increase over the course of cortical rotation, with most dynamic parameters peaking at about 65 minutes post-fertilization. However, many of these parameters did not become significantly elevated until after cortical rotation was underway, suggesting they occur in response to it (see above). The most robust difference we find during the onset of cortical rotation is the large increase in nucleation of plus ends from 35–45 minutes post-activation. Dynein-Dynactin1 interactions have been implicated in microtubule assembly early in cortical rotation (Marrari et al., 2004) and Dctn1 can nucleate microtubules (Ligon et al., 2003), suggesting that Dctn1 might drive the dramatic increase in plus ends following the onset of rotation. Also, the parameters related to growth and shrinkage length best correlated with the establishment of directionality, suggesting that regulation of numbers and length of plus ends by other plus end regulators might account for much of microtubule assembly during cortical rotation.

Our data suggest a model whereby internalization of the array and initiation of cortical rotation are closely coupled, following a buildup of microtubule numbers and dynamicity (Fig. 8). Plus ends then remain anchored in the cortex and are polarized dorsally by the drag of the minus ends and lagging microtubule bundles that are swept up in the shear zone and pulled in the opposite direction. Shear forces may break and shorten misaligned microtubules, creating new sites for growth. We also found a weak bias in plus end growth direction early in rotation, opposite to the eventual direction of alignment, which might provide a directional cue prior to formation of the shear zone. This observation warrants further investigation. Overall, these observations thus provide a useful platform for continuing to investigate the establishment of presumptive dorsal ventral polarity in the egg.

We also used the approaches developed here to investigate the molecular mechanisms of Trim36 in cortical rotation. We suggest that Trim36 is likely to have a coordinating role in microtubule polymerization. Plus end growth speed is greatly increased upon depletion of Trim36, whereas growth lifetime is reduced. Trim36 and related tripartite motif containing subfamily proteins are localized to microtubules and exhibit ubiquitin ligase activity (Meroni and Diez-Roux, 2005); in the case of Trim36, this activity is involved in regulating cortical rotation (Cuykendall and Houston, 2009). The targets of Trim36 ubiquitylation in this context are not yet known, but based on our results we might predict Trim36 to promote the degradation of positive effectors of polymerization. These could include widely characterized proteins like Ckap5/Xmap215, Clip1/Clip170 or Clasp1, although there is no evidence these are ubiquitylated. Interestingly, *trim36* RNA is localized to the mitotic spindle in Xenopus egg extracts and knockdown of Trim36 in cultured cells disrupts spindle organization (Sharp et al., 2011), suggesting a broad role for Trim36 in regulating microtubule dynamics.

Understanding the mechanisms driving cortical rotation will additional insight into the assembly of large-scale microtubule arrays in cells. In animals this is understood largely only with respect to the spindle. The accessibility of the Xenopus oocyte and egg cortex offers good opportunities for investigating general microtubule mechanics in vivo.

Materials and Methods

Plasmids

The *emtb-3xgfp/pcs2+* and *emtb-2xmCherry/pcs2+* plasmids were gifts from W. Bement (University of Wisconsin, Madison, WI), and the *eb3-gfp/pcs2+* was a gift from J. Wallingford (University of Texas at Austin, Austin, TX). Template DNAs for sense transcription from pCS2-derived plasmids was prepared by *Not*I digestion and cleaned by proteinase K digestion. Capped messenger RNA was synthesized using SP6 mMessage mMachine kits according to the manufacturer's instructions (Ambion).

Oocytes and eggs

Ovary was surgically removed from anesthetized *Xenopus laevis* females (wildtype), trimmed into segments and stored at 18°C. Oocytes were manually defolliculated in a modified oocyte culture medium (OCM; 70% L-15 [containing 2 mM 1-glutamine], 0.04% BSA, lx penicillin-streptomicin, pH 7.6–7.8; (Olson et al., 2012) and cultured at 18°C. In some experiments, polyvinyl alcohol (PVA, 0.05%) was substituted for BSA to prevent oocytes from sticking to plastic, with equivalent results. Oocytes were injected vegetally with mRNAs in doses indicated in the text and incubated at 18°C. For oocyte maturation and subsequent prick-activation, oocytes were treated with 2 μM progesterone for 18–22 hours. Mature eggs were transferred to 2% Ficoll 400 (GE Healthsciences) in 0.3 × MMR for 5 minutes and pricked near the animal pole with an empty microinjection needle.

Antisense oligos and host transfer

Antisense oligodeoxynucleotides (oligos) against were HPLC purified phosphorothioate-phosphodiester chimeric oligos (IDT; *trim36*-3: 5′ C*T*TCCAGGTGTCGATG*C*T 3′; Houston and Cuykendall, 2009; *= Phosphorothioate linkages). Oligos were dissolved in nuclease-free water to a concentration of 1.0 mM (~4–5 mg/ml), aliquoted and stored at minus 80°C. Prior to microinjection, oligos were diluted to the appropriate concentration in nuclease-free water and briefly centrifuged to remove any particulate material. Oocytes were injected in the vegetal pole with 4 ng of oligo and cultured for 24 hours at 18°C before being matured by treatment with 2 μM progesterone. Matured oocytes were colored with vital dyes, transferred to egg-laying host females, recovered and fertilized essentially as described (Olson et al., 2012). Females were stimulated to ovulate by injection of hCG (1000 U; Sigma). Eggs were fertilized using a sperm suspension and embryos were reared in 0.1× MMR (1× MMR; 100 mM NaCl, 1.8 mM KCl, 2.0 mM $CaCl_2$, 1.0 mM $MgCl_2$, 15 mM HEPES, pH 7.6). Eggs underwent first cleavage at around 100 minutes after fertilization and thus post-fertilization times are equivalent to normalized times presented in some literature. Embryos were staged according to Nieuwkoop and Faber (1956).

Microscopy and time lapse imaging

Microscopy was performed at room temperature on inverted, wide-field epifluorescence microscopes (DMI4000B, Leica (Fig. 1) or DeltaVision, Applied Precision) using oil-immersion Leica 100×/1.30 N.A. PLANAPO or Olympus 100×/1.40 N.A., UPLS APO UIS2 objectives. Images were acquired using monochrome digital cameras (DFC3000G camera, Leica, or CoolSNAP_HQ2 camera, Photometrics) and Leica AF6000 (64 bit) or SoftWoRx 5.0.0 software (Applied Precision). The pixel size was 0.0644 × 0.0644 × 0.200 μm and image size was 512 × 512 pixels. Time lapse images were collected at two or ten-second intervals. Exposure times were approximately 0.30 seconds on FITC and/or TRITC channels. Samples were kept in either OCM or Ficoll solution for imaging; these were placed in custom aluminum chamber slides cut to the size of a standard microscope slide. Cover slips were attached to the bottom of the wells (1 cm diameter) with nail polish. Images were taken at or near the vegetal pole. In these experiments, the surface of the egg adheres to the coverslip and relative motion is seen as translocation of the cytoplasmic core.

Image processing and quantitation

Movies were initially processed in ImageJ 1.64m (64-bit). Channels were merged when appropriate, and individual frames from plus end movies were exported for plusTipTracker analysis. Consecutive frame averaging and kymograph analysis were performed in ImageJ using the Time Series Painter (van der Vaart et al., 2011) and Multiple Kymograph plugins, respectively. Plus end tracking analysis was performed using plusTipTracker 1.1.4 as described (Applegate et al., 2011), running on MATLAB_R2012a. Detection was by anisotropic Gaussian filtering. Parameters were statistically analyzed using the plusTipTracker group analysis function or using one-way ANOVA in Matlab. Circular statistical analyses were performed using the CircStat toolbox for Matlab (Berens, 2009), which was called from within plusTipTracker by inserting a custom script (available upon request). Images were prepared for publication in ImageJ and Adobe Photoshop and Illustrator; only minor levels and contrast adjustments were made and applied uniformly to the entire image. Other modifications included resizing and changes to stroke/fill weights and colors and the addition of annotation overlays.

Online supplementary material

Videos 1 and 2 shows total microtubules and plus ends in an oocyte and egg, respectively (related to Fig. 1). Fig. SI shows the results of EB3-GFP comet detection. Videos 3 and 4 show long time lapse imaging (10s frame rate, ~25 minutes) of cortical rotation in activated eggs, showing microtubule and plus ends, respectively (related to Fig. 3). Video 5 is a composite video of plus ends at different time points during cortical rotation (related to Fig. 4). Video 6 shows a long time lapse (2s frame rate, ~30 minutes) of cortical rotation in a host-transferred egg (related to Fig. 6). Fig. S2 shows an example of starburst disassembly. Fig. S3 is an example of embryos derived from oocytes expressing EB3 and EMTB, showing normal phenotype. Videos 7 and 8 show microtubules and plus ends in control and *trim36*-depleted embryos, respectively.

Supplementary Material

Refer to Web version on PubMed Central for supplementary material.

Acknowledgments

The authors would like to thank W. Bement and J. Wallingford for reagents and members of the Houston lab for critical reading of the manuscript. We also acknowledge Jing (Lily) Jia for expert technical assistance and Katie Cranston and Abby J. Matthews for early contributions to this project. This work was supported by The University of Iowa and by a grant from the NIH, R01GM083999 to D.W.H.

References

Applegate KT, Besson S, Matov A, Bagonis MH, Jaqaman K, Danuser G. plusTipTracker: Quantitative image analysis software for the measurement of microtubule dynamics. J Struct Biol. 2011; 176:168–184.10.1016/j.jsb.2011.07.009 [PubMed: 21821130]

Batschelet, E. Circular Statistics in Biology. Academic Press; 1981.

Berens P. CircStat: a MATLAB toolbox for circular statistics. J Stat Softw. 2009

Chan AP, Kloc M, Larabell CA, LeGros M, Etkin LD. The maternally localized RNA fatvg is required for cortical rotation and germ cell formation. Mech Dev. 2007; 124:350–363.10.1016/j.mod.2007.02.001 [PubMed: 17376659]

Charbonneau M, Picheral B. Early events in anuran amphibian fertilization: an ultra-structural study of changes occurring in the course of monospermic fertilization and artificial activation. Dev Growth Differ. 1983; 25:23–37.

Clarke EJ, Allan VJ. Cytokeratin intermediate filament organisation and dynamics in the vegetal cortex of living Xenopus laevis oocytes and eggs. Cell Motil Cytoskeleton. 2003; 56:13–26.10.1002/cm.10131 [PubMed: 12905528]

Cuykendall TN, Houston DW. Vegetally localized Xenopus trim36 regulates cortical rotation and dorsal axis formation. Development. 2009; 136:3057–3065.10.1242/dev.036855 [PubMed: 19675128]

Elinson RP. Changes in levels of polymeric tubulin associated with activation and dorsoventral polarization of the frog egg. Dev Biol. 1985; 109:224–233. [PubMed: 3987962]

Gard DL, Kirschner MW. Microtubule assembly in cytoplasmic extracts of Xenopus oocytes and eggs. J Cell Biol. 1987; 105:2191–2201. [PubMed: 3680377]

Ge X, Grotjahn D, Welch E, Lyman Gingerich J, Holguin C, Dimitrova E, Abrams EW, Gupta T, Marlow FL, Yabe T, Adler A, Mullins MC, Pelegri F. Hecate/Grip2a acts to reorganize the cytoskeleton in the symmetry-breaking event of embryonic axis induction. PLoS Genet. 2014; 10:e1004422.10.1371/journal.pgen.1004422 [PubMed: 24967891]

Gerhart J, Danilchik M, Doniach T, Roberts S, Rowning B, Stewart R. Cortical rotation of the Xenopus egg: consequences for the anteroposterior pattern of embryonic dorsal development. Development. 1989; 107(Suppl):37–51. [PubMed: 2699856]

Gerhart, J. Symmetry breaking in the egg of Xenopus laevis. In: Stern, C., editor. Gastrulation: from cells to embryo. 2004. p. 341-351.

Govindan B, Vale RD. Characterization of a microtubule assembly inhibitor from Xenopus oocytes. Cell Motil Cytoskeleton. 2000; 45:51–57. doi:10.1002/. [PubMed: 10618166]

Hebard CN, Herold RC. The ultrastructure of the cortical cytoplasm in the unfertilized egg and first cleavage zygote of Xenopus laevis. Experimental Cell Research. 1967

Houliston E. Microtubule translocation and polymerisation during cortical rotation in Xenopus eggs. Development. 1994; 120:1213–1220.

Houliston E, Elinson RP. Patterns of microtubule polymerization relating to cortical rotation in Xenopus laevis eggs. Development. 1991; 112:107–117. [PubMed: 1769322]

Houston DW. Cortical rotation and messenger RNA localization in Xenopus axis formation. WIREs Developmental Biology. 2012; 1:371–388.10.1002/wdev.29 [PubMed: 23801488]

Jessus C, Thibier C, Ozon R. Levels of microtubules during the meiotic maturation of the Xenopus oocyte. J Cell Sci. 1987; 87(Pt 5):705–712. [PubMed: 3667725]

Jesuthasan S, Stähle U. Dynamic microtubules and specification of the zebrafish embryonic axis. Current Biology. 1997; 7:31–42. [PubMed: 9024620]

Klymkowsky MW, Maynell LA, Polson AG. Polar asymmetry in the organization of the cortical cytokeratin system of Xenopus laevis oocytes and embryos. Development. 1987; 100:543–557. [PubMed: 2443336]

Larabell C, Rowning B, Wells J, Wu M, Gerhart J. Confocal microscopy analysis of living Xenopus eggs and the mechanism of cortical rotation. Development. 1996; 122:1281–1289. [PubMed: 8620855]

Ligon LA, Shelly SS, Tokito M, Holzbaur ELF. The microtubule plus-end proteins EB1 and dynactin have differential effects on microtubule polymerization. Mol Biol Cell. 2003; 14:1405–1417.10.1091/mbc.E02-03-0155 [PubMed: 12686597]

Lu F-I, Thisse C, Thisse B. Identification and mechanism of regulation of the zebrafish dorsal determinant. Proceedings of the National Academy of Sciences. 2011; 108:15876–15880.10.1073/pnas.1106801108

Mandato CA, Bement WM. Actomyosin transports microtubules and microtubules control actomyosin recruitment during Xenopus oocyte wound healing. Current Biology. 2003; 13:1096–1105. [PubMed: 12842008]

Marrari Y, Rouvière C, Houliston E. Complementary roles for dynein and kinesins in the Xenopus egg cortical rotation. Dev Biol. 2004; 271:38–48.10.1016/j.ydbio.2004.03.018 [PubMed: 15196948]

Marrari Y, Clarke EJ, Rouvière C, Houliston E. Analysis of microtubule movement on isolated Xenopus egg cortices provides evidence that the cortical rotation involves dynein as well as Kinesin Related Proteins and is regulated by local microtubule polymerisation. Dev Biol. 2003; 257:55–70. [PubMed: 12710957]

Marrari Y, Terasaki M, Arrowsmith V, Houliston E. Local inhibition of cortical rotation in Xenopus eggs by an anti-KRP antibody. Dev Biol. 2000; 224:250–262.10.1006/dbio.2000.9773 [PubMed: 10926764]

Matov A, Applegate K, Kumar P, Thoma C, Krek W, Danuser G, Wittmann T. Analysis of microtubule dynamic instability using a plus-end growth marker. Nat Methods. 2010; 7:761–768.10.1038/nmeth.1493 [PubMed: 20729842]

Mayr MI, Hümmer S, Bormann J, Grüner T, Adio S, Woehlke G, Mayer TU. The Human Kinesin Kif18A Is a Motile Microtubule Depolymerase Essential for Chromosome Congression. Curr Biol. 17:488–498. [PubMed: 17346968]

Mei W, Jin Z, Lai F, Schwend T, Houston DW, King ML, Yang J. Maternal Dead-End1 is required for vegetal cortical microtubule assembly during Xenopus axis specification. Development. 2013; 140:2334–2344.10.1242/dev.094748 [PubMed: 23615278]

Meroni G, Diez-Roux G. TRIM/RBCC, a novel class of “single protein RING finger” E3 ubiquitin ligases. Bioessays. 2005; 27:1147–1157.10.1002/bies.20304 [PubMed: 16237670]

Miller AL, Bement WM. Regulation of cytokinesis by Rho GTPase flux. Nat Cell Biol. 2009; 11:71–77.10.1038/ncb1814 [PubMed: 19060892]

Mitchison T, Kirschner M. Dynamic instability of microtubule growth. Nature. 1984; 312:237–242. [PubMed: 6504138]

Nieuwkoop, PD.; Faber, J. A systematical and chronological survey of the development from the fertilized egg till the end of metamorphosis. 1. North-Holland Publishing Company; Guilders, Amsterdam: 1956. Normal table of Xenopus laevis (Daudin).

Nojima H, Rothhamel S, Shimizu T, Kim CH, Yonemura S, Marlow FL, Hibi M. Syntabulin, a motor protein linker, controls dorsal determination. Development. 2010; 137:923–933.10.1242/dev.046425 [PubMed: 20150281]

Olson DJ, Hulstrand AM, Houston DW. Maternal mRNA Knock-down Studies: Anti-sense Experiments Using the Host-Transfer Technique in Xenopus laevis and Xenopus tropicalis. Methods Mol Biol. 2012; 917:167–182.10.1007/978-1-61779-992-1_10 [PubMed: 22956088]

Pierre P, Scheel J, Rickard JE, Kreis TE. CLIP-170 links endocytic vesicles to microtubules. Cell. 1992; 70:887–900.10.1016/0092-8674(92)90240-D [PubMed: 1356075]

Robb DL, Heasman J, Raats J, Wylie CC. A kinesin-like protein is required for germ plasm aggregation in Xenopus. Cell. 1996; 87:823–831. [PubMed: 8945510]

Schroeder MM, Gard DL. Organization and regulation of cortical microtubules during the first cell cycle of Xenopus eggs. Development. 1992; 114:699–709. [PubMed: 1618137]

Sharp JA, Plant JJ, Ohsumi TK, Borowsky M, Blower MD. Functional analysis of the microtubule-interacting transcriptome. Mol Biol Cell. 2011; 22:4312–4323.10.1091/mbc.E11-07-0629 [PubMed: 21937723]

Strähle U, Jesuthasan S. Ultraviolet irradiation impairs epiboly in zebrafish embryos: evidence for a microtubule-dependent mechanism of epiboly. Development. 1993; 119:909–919. [PubMed: 8187646]

Tran LD, Hino H, Quach H, Lim S, Shindo A, Mimori-Kiyosue Y, Mione M, Ueno N, Winkler C, Hibi M, Sampath K. Dynamic microtubules at the vegetal cortex predict the embryonic axis in zebrafish. Development. 2012; 139:3644–3652.10.1242/dev.082362 [PubMed: 22949618]

Trimble L, Fluck R. Indicators of the dorsoventral axis in medaka (Oryzias latipes) zygotes. The Fish Biology Journal. 1995; 7:37–41.

van der Vaart B, Manatschal C, Grigoriev I, Olieric V, Gouveia SM, Bjelic S, Demmers J, Vorobjev I, Hoogenraad CC, Steinmetz MO, Akhmanova A. SLAIN2 links microtubule plus end-tracking proteins and controls microtubule growth in interphase. J Cell Biol. 2011; 193:1083–1099.10.1083/jcb.201012179 [PubMed: 21646404]

Weaver C, Kimelman D. Move it or lose it: axis specification in Xenopus. Development. 2004; 131:3491–3499.10.1242/dev.01284 [PubMed: 15262887]

Highlights

- Microtubule dynamics are monitored in Xenopus oocytes and fertilized eggs.
- Rapid microtubule plus end flux in oocytes and stable polymeric tubulin.
- Polarization of plus ends is rapid following onset of cortical rotation.
- Nascent microtuble network subduction into deep yolk prior to cortical rotation.
- Vegetally-localized Trim36 coordinately regulates plus end dynamics.

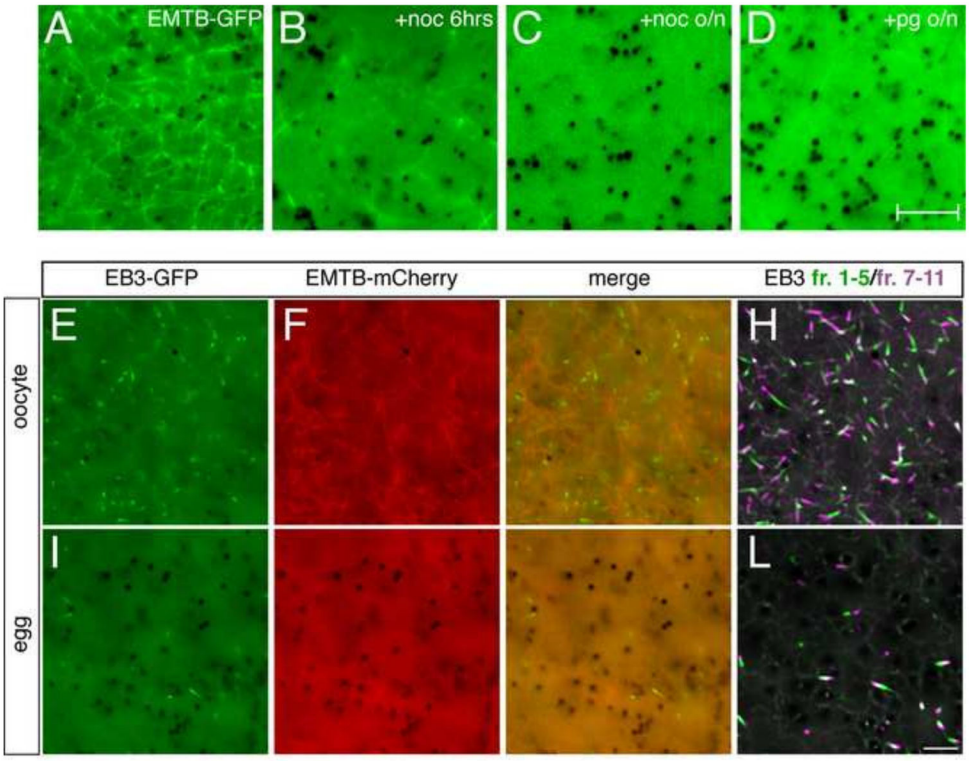

Fig. 1. Reduced cortical microtubule stability and plus end growth during the oocyte-to-egg transition

(A–D) Representative images of oocytes injected with *emtb-3xgfp* (500 pg; vegetal views). (A) Control untreated oocyte. (B) Oocyte treated with nocodozole (+noc, 3.3 nM) for six hours, or (C) overnight. (D) Oocyte treated with progesterone (+pg, 2 μM) overnight to induce oocyte maturation. (E–H) Oocytes or (I–L) eggs (progesterone-treated oocytes) injected with *emtb-mCherry* (500 pg) and *eb3-gfp* (500 pg) mRNAs. (H, L) Individual frames from time-lapse movies of co-injected oocytes and eggs demonstrating EB3-GFP dynamics (Supplementary Videos 1 and 2). To facilitate visualization, frames 1–5 and 7–11 of each movie were averaged, merged and pseudo colored green and magenta respectively, representing 20 seconds of MT plus end growth. Dark structures are pigment granules. Scale bars represent 7.5 μm (A–D) and 5 μm (I–L).

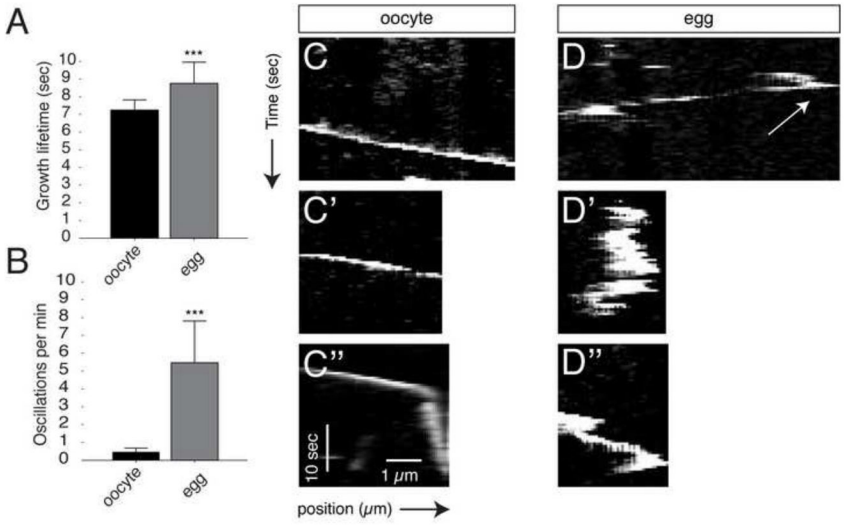

Fig. 2. Plus ends exhibit oscillatory behavior in the cortex of the unactivated egg

(A) Mean plus end growth lifetime. (B) number of plus end oscillations in oocytes and eggs. Error bars represent standard deviations around the mean; *** = p-value < 1.0E-9 (t-test). N=40 in (A), N=10 in (B–D″). (C–C″, D–D″) Representative kymographs of EB3-GFP comets in oocytes and eggs. The arrow in (C) indicates an example of the initiation of rearward oscillation.

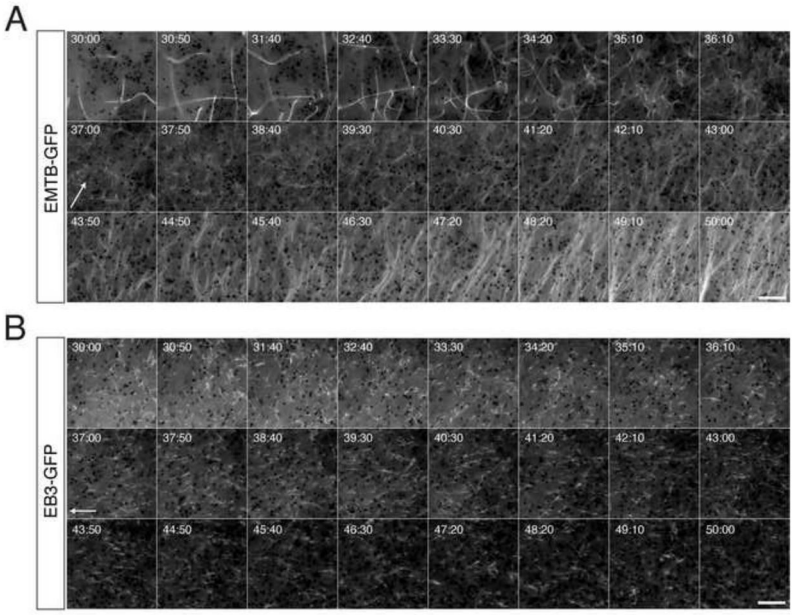

Fig. 3. Time lapse imaging of microtubule assembly and plus end orientation during cortical rotation in activated eggs

(A) Representative time-lapse imaging of a prick-activated egg injected with *emtb-gfp* mRNA (500 pg), or (B) with *eb3-gfp* mRNA (500 pg). Panels in (A) and (B) show selected frames at 50 second intervals from Supplementary Videos 3 and 4, respectively Elapsed time from prick activation is shown at the top of each frame (in mimsec). Arrows indicate the frame of onset and approximate direction of relative movement of the yolk mass. Scale bars = 10 μm.

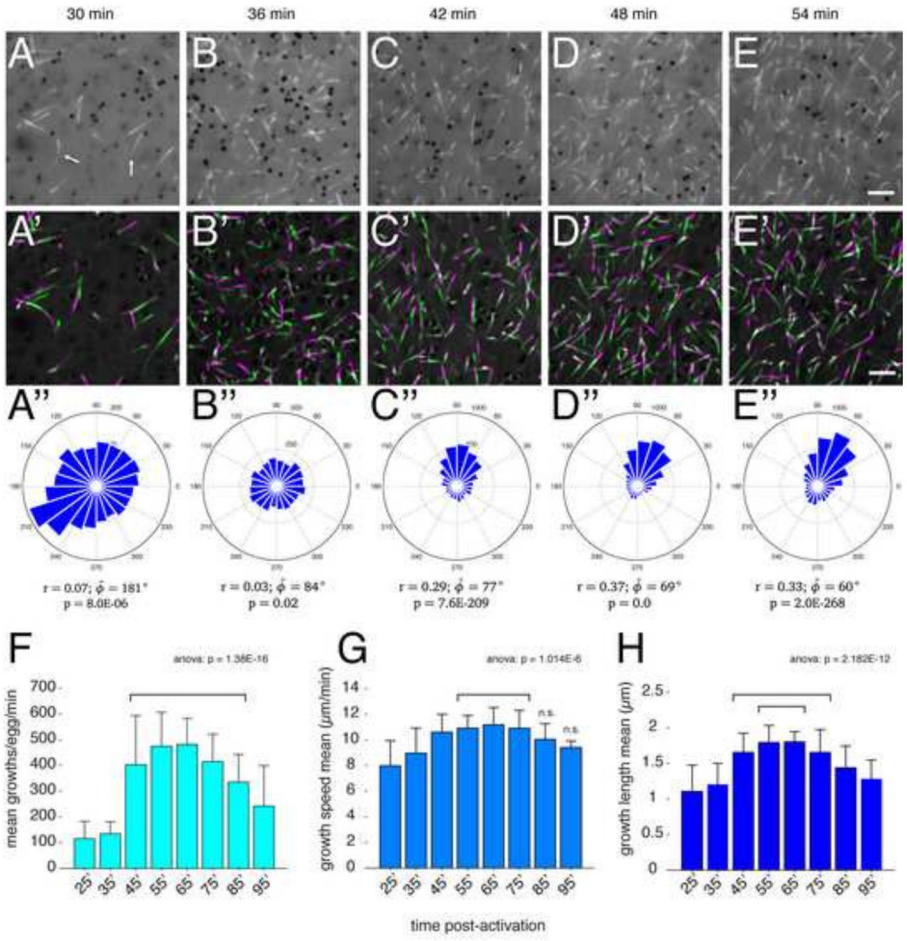

Fig. 4. Changes in microtubule plus end dynamics during cortical rotation in activated eggs

(A–E) Individual frames from time-lapse movies of a representative EB3-GFP-expressing prick-activated egg and the indicated times; (A′–E′) Frames 1–5 and 7–11 of each movie were averaged, merged and pseudo colored green and magenta respectively, representing 20 seconds of MT plus end growth. Arrows in (A) indicate curved and kinked plus end comets. (A″–E″) Angle histogram plots showing the directionality of individual MT plus end tracks. Plots show number of tracks per bin for each two-minute time-lapse movie. Circular statistics for each dataset are shown below the plot, indicating mean resultant vector length (r, where $0 \leq r \leq 1$; 1= concentration at mean angle), mean angle ($\bar{\phi}$, phi_bar) and p-value of the Rayleigh test for circular uniformity. Please note differing scales on the plots. (F–H) Graphs showing mean plus end growth numbers (F), speed (G) and length (H) at the indicated time points; N=21 prick-activated eggs (seven experiments, three eggs per experiment). The p-values from one-way ANOVA are indicated at the top; brackets indicate groups not statistically different from each other but differing from all surrounding groups (excluding n.s.) in post-hoc multiple comparison tests (using Tukey's HSD criterion; n.s.=not significantly different from any group). Scale bar = 5 μm.

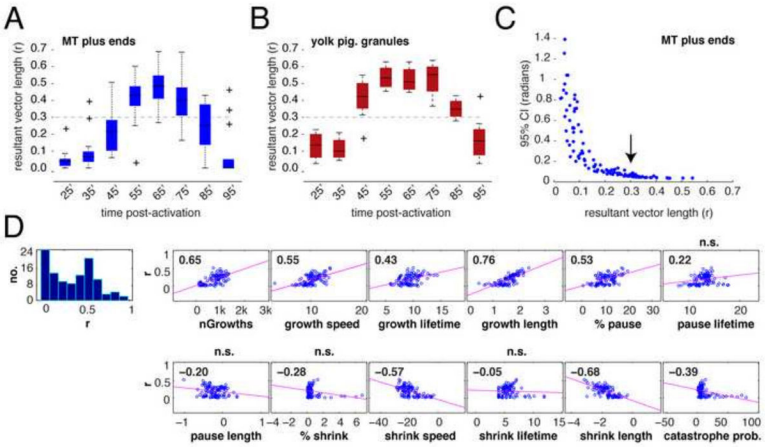

Fig. 5. Microtubule plus end orientation occurs subsequent to the onset of cortical rotation

(A–B) Average r values for MT plus ends (A) and the yolk mass (B); N=21 prick-activated eggs. The dark bar in each box indicates the median r value per group, lower and upper edges of the colored boxes indicate 25th and 75th percentiles respectively, whiskers represent maximum and minimum adjacent values (excluding outliers (+)). The dashed line demarcates the estimated r value at which directionality becomes strongly concentrated (0.3, determined in panel (C)). (C) Scatterplot of mean resultant vector length against the 95% confidence interval (CI). The arrow indicates the value of r where the CI reaches a consistent minimum. (D) Correlation plots of r value against other dynamic parameters. The first panel shows the histogram of mean resultant vector length data, the remaining panels show scatterplots of other variables paired with r. The pink lines indicate the least-squares reference lines; correlation coefficients are shown in each graph panel, n.s. indicates which panels have non-significant p-values for the correlation.

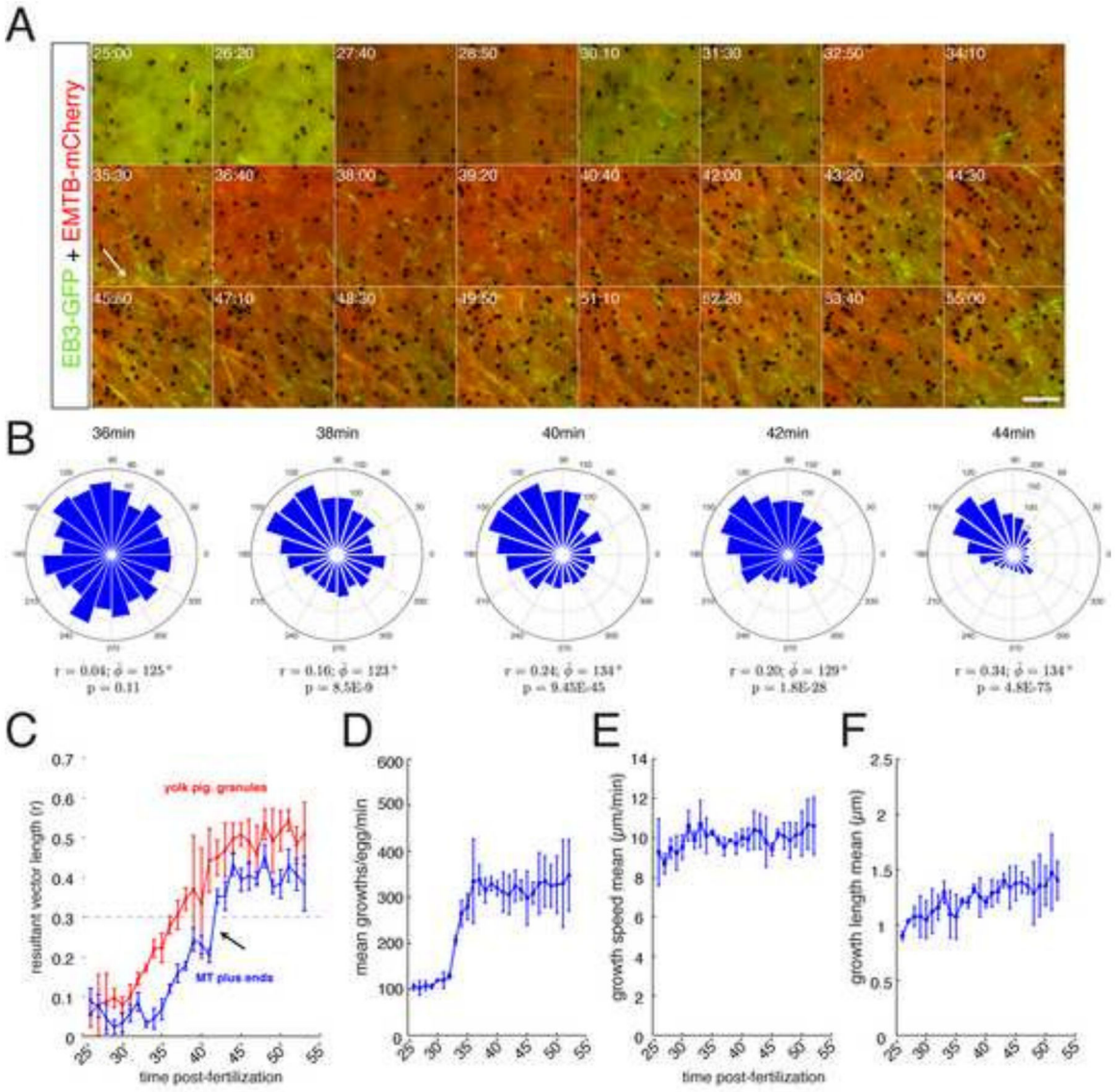

Fig. 6. Time lapse imaging of microtubule assembly and plus end orientation during cortical rotation in fertilized eggs

(A) Representative time-lapse imaging of a zygote obtained by the host-transfer procedure, previously injected as an oocyte with *emtb-gfp* mRNA (500 pg) and *eb3-gfp* mRNA (500 pg). Panels in (A) show selected frames at 80-second intervals from Supplementary Video 6 (30 minute time-lapse, frame rate = 2 seconds). Elapsed time from in vitro fertilization is shown at the top of each frame (in min:sec). The arrow indicates the frame of onset and approximate direction of relative movement of the yolk mass. Scale bar represents 5 μm. (B) Angle histogram plots showing the directionality of individual MT plus end tracks at selected times. Note differing scales. (C) Plots of the strength of directionally of MT plus ends (blue) and yolk pigment granules (red) during the onset of cortical rotation. Data points represent mean resultant vector length obtained from circular statistical analysis of one-minute windows. Brackets indicate standard deviation. (D–F) Plots of selected MT plus end growth parameters. N=four host-transferred eggs, derived from oocytes from two females.

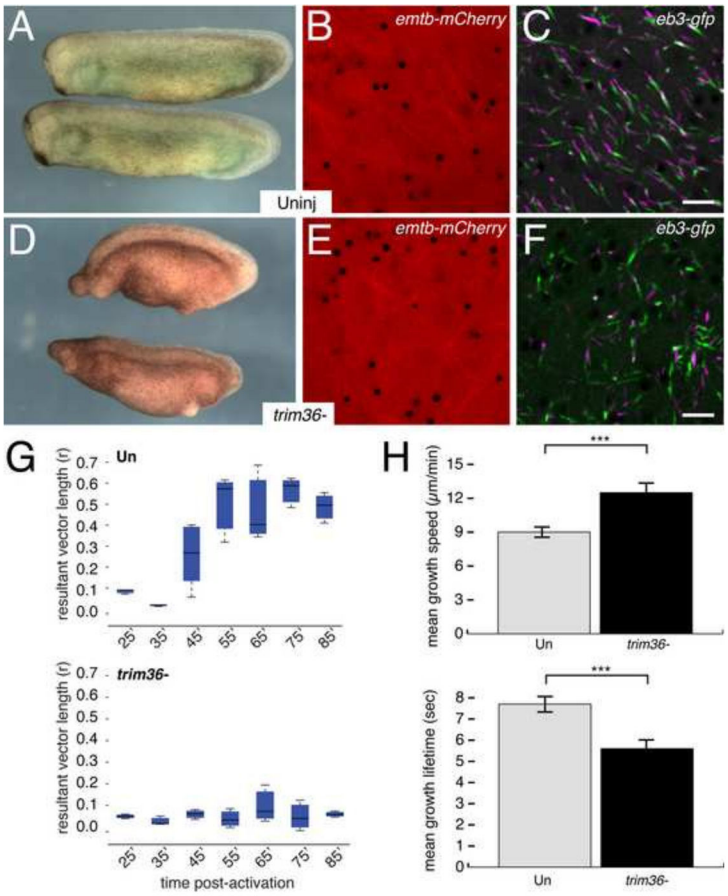

Fig. 7. Disordered microtubule assembly and plus end orientation in *trim36*-depleted embryos

(A, D) Representative control uninjected (Uninj) and *trim36*-depleted (*trim36*-) tailbud stage embryos (stage 28) obtained from host-transfer experiments. Anterior to left, dorsal to top. (B, E) Individual frames from time-lapse movies of *eb3-gfp* + *emtb-mCherry-expressing* eggs, showing EMTB-labeled microtubules ~45 minutes post-activation. (C, F) Averaged, merged and pseudo colored frames of EB3-labeled microtubule plus ends. Frames 1–5 are shown in green; frames 7–11 are in magenta. (Supplementary Videos 7 and 8). (G) Average r values for MT plus ends in uninjected control (upper panel) and *trim36*-depleted (lower panel) eggs. The dark bar in each box indicates the median r value per group, lower and upper edges of the colored boxes indicate 25th and 75th percentiles respectively, whiskers represent maximum and minimum adjacent values. (H) Graphs showing mean plus end growth speed (upper panel) and lifetime (lower panel) in control and *trim36*-depleted eggs (~45 minutes post-fertilization). Error bars indicate standard deviation; *** = $p < 1.0E-4$ (t-test). N=9 prick-activated eggs per group (donor oocytes from three different females). Scale bar = 5 μm (applies to B, C, E, F).

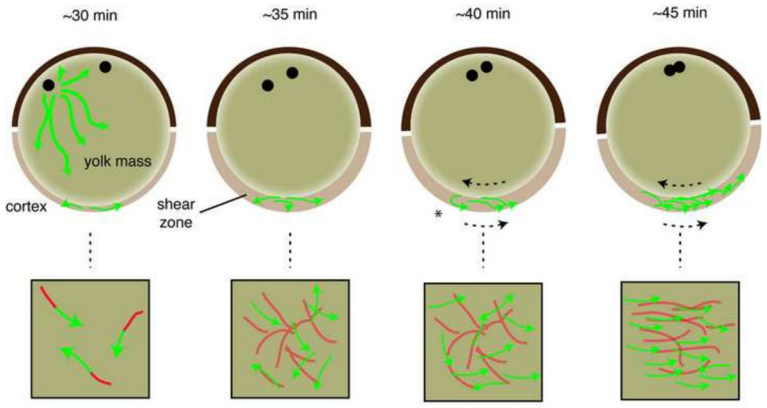

Fig. 8. Model for dorsal microtubule orientation during the initiation of cortical rotation

Microtubules are depolymerized immediately after fertilization (not shown) and begin to polymerize in the cortex by 30 minutes post-fertilization (~30 min). Growing plus ends (green arrows) generate trailing stable microtubules (red). In a more animal position, astral microtubules have assembled around the sperm pronucleus and these may extend vegetally and stimulate or contribute to the growth in the cortex (omitted for clarity in other panels). By 35 minutes post-fertilization (~35 min), the numbers of growing plus ends begins to increase and a dense cortical microtubule network is formed. Around this time, the yolk increases in firmness and the viscosity in the subcortical cytoplasm decreases, creating a fluid shear zone that allows relative movement between the two regions of the egg. This is represented in the model as a thickening in the vegetal region although this is likely occurs throughout the egg. As this occurs, the microtubule network associates with the deeper yolk mass (subduction; represented by lighter shading) and moves with that structure during cortical rotation. There is no obvious bias in plus end orientation at this time. At 40 minutes post-fertilization (~40 minutes), cortical rotation is apparent (dotted arrow indicate relative movement) and plus ends become directionally oriented at this time. We suggest that new growth is oriented because plus ends remain primarily cortical whereas the stabilized body of the microtubule is dragged in the opposite direction by its association with the yolk mass (asterisk). Shear induced shortening of misaligned microtubules may also occur at this time. As plus end growths increase in number, new trailing microtubules would then associate with the moving yolk mass or become aligned by shear and pull the plus ends into alignment (~45 min). The upper images depict sagittal sections of eggs, with the animal pole toward the top and presumptive dorsal to the right. The lower panels represent en face views of the vegetal cortex.

Table 1

Plus end dynamic parameters in oocytes and metaphase II arrested eggs.

	(1) oocyte	(2) egg	adj p-value
Growths per egg per min	344.72 ± 137.00	144.62 ± 69.00	1.56E-06
Growth speed (μm/min)	7.13 ± 1.43	6.60 ± 0.67	0.241
Growth lifetime (sec)	7.25 ± 0.58	8.75 ± 1.19	3.80E-10
Growth length (μm)	0.76 ± 0.18	0.71 ± 0.06	0.507
Percent pause	22.25 ± 4.82	9.18 ± 2.86*	1.22E-09
Pause lifetime (sec)	13.43 ± 1.16	11.64 ± 2.28*	0.00031
Pause length (μm)	−0.49 ± 0.17	−0.117 ± 0.17*	5.00E-08
Percent shrinkage	0.44 ± 0.65	0.24 ± 0.81*	0.00320
Shrinkage speed (μm/min)	−12.23 ± 2.27	−9.58 ± 1.91*	0.02061
Shrinkage lifetime (sec)	7.25 ± 2.48	5.82 ± 1.20*	0.19142
Shrinkage length (μm)	−1.46 ± 0.54	−0.90 ± 0.16*	0.01167
Catastrophe probability (%)	3.14 ± 3.96	3.81 ± 11.08*	0.01392

Time-lapse movies (frame rate = 2 sec) of EB3-GFP dynamics in oocytes and progesterone-treated oocytes (egg) injected with 500 pg *eb3-gfp* mRNA were analyzed using plusTipTracker (Applegate et al., 2011). Values represent means plus or minus the standard deviation (s.d.); N=40 per group. Adjusted p-values following t-tests following multiple comparison correction are shown (Benjamini and Hochberg, 1995; Benjamini and Yekutieli, 2001).

* in the egg group indicates that gap parameters may reflect not the oscillations present in the mature oocyte.

Table 2

Plus end dynamic parameters during cortical rotation in prick-activated eggs.

	(1) 25 min	(2) 35 min	(3) 45 min	(4) 55 min	(5) 65 min	(6) 75 min	(7) 85 min	(8) 95 min	ANOVA	significant groups
Growths/egg/min	115 ± 67.72	134.35 ± 46.66	402.62 ± 190.52	474.36 ± 131.96	481.67 ± 100.30	415.04 ± 106.40	334.96 ± 108.24	241.63 ± 157.02	p = 1.38E-16	1,2,8: 3–7
Growth speed (μm/min)	7.99 ± 1.96	8.97 ± 1.97	10.60 ± 1.39	10.92 ± 0.98	11.18 ± 1.34	10.91 ± 1.39	10.05 ± 1.22	9.41 ± 0.51	p = 1.014E-06	1–3: 4–6
Growth lifetime (sec)	8.64 ± 1.51	8.17 ± 1.16	9.71 ± 2.05	10.03 ± 1.09	9.97 ± 1.64	9.18 ± 1.47	8.82 ± 1.89	8.42 ± 1.38	p = 0.277	n.s.
Growth length (μm)	1.10591 ± 0.37	1.20 ± 0.30	1.65 ± 0.27	1.79 ± 0.24	1.80 ± 0.14	1.65 ± 0.32	1.44 ± 0.31	1.28 ± 0.27	p = 2.182E-12	1,2,7,8: 3–6; 1–3,6–8: 4,5
Time in pause (%)	9.09 ± 3.55	6.73 ± 4.78	9.24 ± 3.49	11.63 ± 3.79	12.37 ± 3.55	11.36 ± 2.81	8.57 ± 2.55	4.64 ± 4.04	p = 0.0059	5: 7,8
Pause lifetime (sec)	13.32 ± 2.0	12.42 ± 2.67	12.22 ± 1.883	13.20 ± 0.95	13.11 ± 1.01	12.92 ± 1.00	12.95 ± 1.59	11.25 ± 0.19	p = 0.608	n.s.
Pause length (μm)	−0.28 ± 0.28	−0.23 ± 0.24	−0.26 ± 0.15	−0.29 ± 0.09	−0.23 ± 0.24	−0.20 ± 0.30	−0.051 ± 0.16	−0.22 ± 0.10	p = 0.2926	n.s.
Time in shrinkage (%)	0.86 ± 0.716	1.88 ± 2.77	0.25 ± 0.20	0.34 ± 0.11	0.31 ± 0.25	0.31 ± 0.36	0.18 ± 0.43	1.94 ± 3.74	p = 0.0142	2: 3–7
Shrinkage speed (μm/min)	−10.02 ± 4.28	−12.90 ± 6.19	−21.10 ± 3.24	−21.00 ± 3.15	−22.24 ± 4.21	−23.34 ± 3.40	−21.77 ± 5.42	−19.06 ± 11.61	p = 0.0359	n.s.
Shrinkage lifetime (sec)	6.42 ± 2.16	6.25 ± 2.82	5.31 ± 1.23	5.72 ± 0.69	5.67 ± 1.09	5.32 ± 0.900	4.72 ± 0.85	6.067 ± 3.60	p = 0.3126	n.s.
Shrinkage length (μm)	−0.99 ± 0.39	−1.11 ± 0.45	−1.85 ± 0.52	−1.98 ± 0.36	−2.06 ± 0.50	−2.08 ± 0.62	−1.65 ± 0.42	−1.38 ± 0.59	p = 2.922E-05	1,2,7,8: 3–6; 1–3,6–8: 4,5
Catastrophe probability (%)	16.25 ± 13.45	27.00 ± 30.48	5.70 ± 4.43	6.73 ± 2.84	5.10 ± 2.88	5.53 ± 4.24	5.10 ± 12.09	26.64 ± 48.94	p = 0.017	n.s.

Time-lapse movies (frame rate = 2 sec) of EB3-GFP dynamics in prick-activated eggs injected as oocytes with 500 pg *eb3-gfp* mRNA were analyzed using plusTipTracker (Applegate et al., 2011). Values represent means plus or minus the standard deviation (s.d.); N=21 eggs. P-values from one-way ANOVA are shown, pairs with significant differences in mean are indicated (significant groups; groups to the left of the colon are not different from each other but are different from each group on the right).